Mutation of *wrb*, a Component of the Guided Entry of Tail-Anchored Protein Pathway, Disrupts Photoreceptor Synapse Structure and Function

Lauren L. Daniele,[1] Farida Emran,[2] Glenn P. Lobo,[1] Robert J. Gaivin,[1] and Brian D. Perkins[1]

[1]Department of Ophthalmic Research, Cole Eye Institute, Cleveland Clinic, Cleveland, Ohio, United States
[2]Centre for Research in Neuroscience, McGill University, Montreal, Quebec, Canada

Purpose. Tail-anchored (TA) proteins contain a single hydrophobic domain at the C-terminus and are posttranslationally inserted into the ER membrane via the GET (guided entry of tail-anchored proteins) pathway. The role of the GET pathway in photoreceptors is unexplored. The goal of this study was to characterize the zebrafish *pinball wizard* mutant, which disrupts Wrb, a core component of the GET pathway.

Methods. Electroretinography, optokinetic response measurements (OKR), immunohistochemistry, and electron microscopy analyses were employed to assess ribbon synapse function, protein expression, and ultrastructure in 5-day-old zebrafish larvae. Expression of *wrb* was investigated with real-time qRT-PCR and in situ hybridization.

Results. Mutation of *wrb* abolished the OKR and greatly diminished the ERG b-wave, but not the a-wave. Ribeye and SV2 were partially mislocalized in both photoreceptors and hair cells of *wrb* mutants. Fewer contacts were seen between photoreceptors and bipolar cells in *wrb*$^{-/-}$ mutants. Expression of *wrb* was observed throughout the nervous system and Wrb localized to the ER and synaptic region of photoreceptors. Morpholino knockdown of the cytosolic ATPase *trc40*, which targets TA proteins to the ER, also diminished the OKR. Overexpression of *wrb* fully restored contrast sensitivity in mutants, while overexpression of mutant *wrb*^{R73A}, which cannot bind Trc40, did not.

Conclusions. Proteins Wrb and Trc40 are required for synaptic transmission between photoreceptors and bipolar cells, indicating that TA protein insertion by the TRC pathway is a critical step in ribbon synapse assembly and function.

Keywords: zebrafish, ribbon synapse, optokinetic response, photoreceptors

Rod and cone photoreceptors require multiple mechanisms to ensure that different types of membrane proteins correctly associate with the appropriate membranes, which is a prerequisite for targeting to the appropriate subcellular compartments. During translation, the signal recognition particle (SRP) binds to the majority of integral membrane proteins, such as rhodopsin and the cyclic-nucleotide gated channel, and guides the nascent polypeptides to the endoplasmic reticulum (ER) for membrane insertion. Following membrane insertion, distinct pathways transport these proteins to either disc membranes or the plasma membrane.[1,2] Meanwhile, proteins such as transducin that associate with the membrane via posttranslational lipidation do not require membrane insertion and arrive at the outer segment via a separate Unc119-dependent pathway.[3–5] Hundreds of membrane proteins, including SNARE proteins and the RGS9-anchor protein (R9AP), attach to the membrane by a single transmembrane domain located at the C-terminus. These tail-anchored (TA) proteins are not recognized by the SRP during translation and must be inserted in the ER membrane by posttranslational pathways, the best known being the guided-entry of TA protein insertion (GET) pathway.[6] Little is known about the mechanisms necessary for membrane incorporation of these numerous TA proteins.

Mechanistic studies of the GET pathway in yeast demonstrated that the cytoplasmic ATPase Trc40 recognizes the transmembrane domain of TA proteins and delivers the proteins to the ER. Next, the proteins Wrb (tryptophan-rich basic protein) and its coreceptor calcium-modulating cyclophilin ligand (CAML) recruit Trc40 to the ER,[7,8] where they stimulate the ATP-dependent release of nascent TA cargo from Trc40 and facilitate ER membrane insertion.[9] Despite the biochemical characterization and mechanistic insight into the GET pathway in yeast, the in vivo requirements for the GET pathway in vertebrates remain unclear. Targeted deletion of *Trc40* or *Caml* resulted in embryonic lethality between embryonic day (E)-3.5 and −8.5 in mice,[10,11] while morpholino knockdown of *Xenopus wrb*, also known as congenital heart disease protein 5 (*cdh5*), disrupted heart development.[12]

In a forward genetic screen for zebrafish with visual function deficits, we previously identified *wrb*^{bi1482}, a mutant with a retroviral insertion.[13] Zebrafish *wrb*$^{-/-}$ mutants had reduced visual function resulting from disordered connections between photoreceptors and bipolar cells. Ribbon architecture was relatively intact, but fewer bipolar cell dendrites invaginated into cone pedicles. Disrupting Trc40 expression also reduced visual function and disrupted synaptic contacts. Visual function was lost when the interaction between Wrb and Trc40 was

blocked by mutation of a conserved coiled-coil domain of Wrb. Finally, visual behavior was restored when *wrb* was expressed in cone photoreceptors. Together these results reveal that photoreceptor synapse architecture and function requires an intact GET pathway.

MATERIALS AND METHODS

Zebrafish Maintenance

Zebrafish were maintained on Aquatic Habitats (Apopka, FL, USA) recirculating water systems in a 14/10-hour light/dark cycle. All experimental procedures were approved by the Cleveland Clinic Institutional Animal Care and Use Committee. The mutant *wrb^{bi1482}* was initially identified in a forward genetic screen for mutants affecting ocular development or function.[13] The transgenic line *Tg(UAS:gap43-YFP)q16b; Tg(nyx:Gal4-VP16)^{q16a}*,[14] which we will refer to as Tg(nyx:mYFP), was obtained from James Fadool (Florida State University). We confirm that all experiments adhered to the ARVO Statement for the Use of Animals in Ophthalmic and Vision Research.

Transgene Generation

The transgenic line *Tg(−3.2gnat2:wrb-eGFP)^{fri48Tg}*, which we will refer to as the *Tg(TαC:wrb-eGFP)*, was generated using Tol2 transgenesis and the Gateway Tol2 kit.[15] Briefly, the *wrb* cDNA was cloned by RT-PCR from 5 days post fertilization (dpf) zebrafish larvae with the primers 5′-GGGGACAAGTTTGTA CAAAAAGCAGGCTTCATGGCTGCCGGGTTTAAC-3′ and 5′-GGGGACCACTTTGTACAAGAAAGCTGGGTCACTGACAGCTT GTAGAATGAGGG-3′ and recombined into the gateway vector pENTR221. The vector p5E-TαCP encoding the zebrafish cone transducin promoter[16] was provided by Susan Brockerhoff (University of Washington, Seattle, WA, USA).

Genotyping

Genotyping was performed by duplex PCR using a single forward primer annealing to exon1 of both mutant and WT *wrb* 5′-TGTGTTTCTGTGCAACCTCG-3′, as well as a reverse strand primer 5′-TTGTTCGCTGTGCCTACAAGAAG-3′ annealing to WT intron 1 sequence and 5′-GCTCAATAAAAGAGCC CACAACC-3′ annealing to the intronic retroviral insert in *wrb^{bi1482}* mutants.

Touch Response Assay

We screened *wrb^{bi1482}* mutants at 5 dpf by an abnormal response to light touch with an insect pin. Responses from larvae selected randomly were classified on a 0 to 3 scale: 0, assigned to trials where touch did not elicit a response; 1, response to touch was sluggish; 2, response was to swim away vigorously; 3, larvae darted away before the tail could be touched. Responses rated 0 or 1 were classified as abnormal; responses rated 2 and 3 were classified as normal.

qPCR and In Situ Hybridization

Real-time PCR was performed with a commercial system (CFX96; Bio-Rad Laboratories, Hercules, CA, USA) using SYBR green detection (SYBR green supermix; Bio-Rad Laboratories) and the following probes:

Wrb: 5′-TGTGTTTCTGTGCAACCTGC-3′ and 5′-CAGTCCT CATCTCCATCTCCTG-3′; and

β-actin: 5′-TTTTGTACTTCAGCCTTAAACTTGG-3′ and 5′-AGTCCTGCAAGATCTTCACTTTTTA-3′

Values given are relative quantities normalized to *b-actin* expression. Estimates of *wrb* expression in 5 dpf *wrb^{+/−}* and *wrb^{−/−}* relative to WT were based on seven and four datasets respectively.

In situ hybridization was performed on fixed 5 dpf larvae as described.[17] Antisense and sense probes were transcribed from *wrb* cDNA in pCS2+8 with T7 and SP6 polymerases, respectively.

Synthesis of mRNA for Rescue Experiments

Zebrafish *wrb* and human *TRC40* cDNAs were cloned from larvae or hTERT cell total RNA using RT-PCR (Superscript II first strand synthesis; Life Technologies, Carlsbad, CA, USA). Untagged wrb was ligated into pCS2+8 from an RT-PCR amplified with the primers: 5′-TAAGCAGAATTCCCAC CATGGCTGCCGGGTTTAAC-3′ and 5′-TGCTTACTCGAGT TAACTGACAGCTTGTAGAATGAGGGC-3′. A codon switch encoding the *wrb^{R73A}* mutation was introduced into *wrb* in pENTR221 by site directed mutagenesis (GENEART; Life Technologies) using the primers 5′-GCCAGATATGCTAGACTG GAAGAAAAGATCAACAAGATGACTGAT-3′ and 5′-ATCAGT CATGTTGATCTTGGCTTCCAGTCTAGCATATCTGGC-3′. Gateway recombination into pDESTTOL2pA2 incorporated a GFP tag onto *wrb* and *TRC40*. We synthesized 5′-capped mRNAs encoding human *TRC40-eGFP, wrb, wrb^{R73A}*-eGFP, and *wrb-eGFP* from plasmid vectors using a transcription kit (mMessage mMachine; Ambion/Life Technologies) with SP6 polymerase. For mRNA rescue of morphants, the mRNA solution was injected into a population of 1 to 2 cell embryos injected with morpholino.

Morpholino Injections

Morpholino antisense oligonucleotides targeting the translation start site (TCTTCCACTGAAGCTGCCATCTTGC) or the exon3-intron3 splice junction of *trc40* (GCCTTGAA CGCGAGTCTGACCTCAT; Genetools, Philomath, OR, USA) were diluted to 3–8 ng/nL in 1X Danieau's solution and injected into 1-cell stage embryos.

Electroretinography

Electroretinography was performed on isolated larval eyes (at 5 dpf) as previously described.[18] Briefly, larvae were dark-adapted for 1 hour, euthanized, and eyes removed with tungsten wire and kept moist by placement on 2% agarose with continuous superfusion with Ringer's. We bubbled Ringer's with 97% O_2 3% CO_2 to maintain pH 7.8. Sweeps of ERG were extracted and analyzed with custom scripts using data analysis software (IgorPro; WaveMetrics, Portland, OR, USA). For drug treatments, 100 mM stocks of threo-beta-benzyloxyaspartate (TBOA; Tocris Biosciences, Minneapolis, MN, USA) and L-2-amino-4-phosphonobutyric acid (L-AP4; Sigma-Aldrich Corp., St. Louis, MO, USA) were made in DMSO and 0.1 M NaOH, respectively. Larvae were placed in fish water containing 0.2 mM TBOA and 0.4 mM L-AP4 for 2 hours prior to ERG recording.

Optokinetic Response (OKR) Measurements

The measurements of OKR were made with the oculomotor analysis system[19] (VisioTracker; Tse Systems GmbH, Bad Homburg vor der Höhe, Germany). Zebrafish larvae were immobilized in 3% methylcellulose in a 35-mm petri dish and placed in the oculomotor analysis system (Tse Systems GmbH). Saccades were quantified from larvae presented with a unidirectional stimulus

moving at a constant speed for approximately 1 minute. To measure contrast response functions, the direction of the stimulus was alternated every 3 seconds. The spatial frequency (0.06 cyc/deg) and speed (7.5 degrees/s) of the vertical stripe pattern were held constant and stepwise decrements and increments to contrast were made. Contrast sensitivity was measured using gain (the ratio of angular velocities of eye versus stimulus) as a function of log contrast percentage.[20]

Immunohistochemistry and Fluorescence Imaging

Larvae were euthanized and fixed at 4°C overnight in 4% paraformaldehyde in 1X PBS. Larvae were cryoprotected by incubation at 4°C in 30% sucrose in 1X PBS for at least 8 hours. Cryosections (10–15 μm) were placed on gelatin coated slides and blocked 1 hour at room temperature prior to an overnight incubation with primary antibodies. Blocking solution consisted of 1% BSA, 10% normal goat serum (NGS), 0.5% Triton X-100, in 1× PBS. Whole larvae were fixed for 2 hours in 4% paraformaldehyde prepared in 1X PBS, then permeabilized for 1 hour at 4°C with 0.5% Triton X-100 in fixative, followed by blocking in 2% NGS, 1% BSA, 1% DMSO, 1X PBS. Antibodies were diluted in blocking buffer without normal serum. The following antibodies were used: calcium channel Cav1.4α (1:3000; Michael Taylor, St. Jude Children's Research Hospital, Arlington, VA, USA); syntaxin3 (1:100; Synaptic Systems, Atlanta, GA, USA); ribeye b (1:500; Teresa Nicolson, Oregon Health & Science University, Portland, OR, USA); Zpr-1 (1:200; Zebrafish International Resource Center); SV2 (1:200; monoclonal antibody developed by Kathleen M. Buckley, Harvard Medical School; Maintained by Developmental Studies Hybridoma Bank University of Iowa). AlexaFluor 488 and AlexaFluor 568 conjugated secondary antibodies were purchased from Invitrogen Life Technologies. Optical sections were obtained with a fluorescent microscope fitted with for structured illumination (Zeiss Axio Imager.Z2 with Apotome.2; Carl Zeiss Microscopy, Thornberg, NY, USA). Image panels were created with ImageJ (http://imagej.nih.gov/ij/; provided in the public domain by the National Institutes of Health, Bethesda, MD, USA).[21]

Live DASPEI Labeling

Larval zebrafish (5 dpf) were incubated in a solution of DASPEI diluted to 0.01% with 0.06% tricaine at 28.5°C for 10 minutes, then washed several times in fish water containing tricaine. Fish that were DASPEI-labeled were imaged with fluorescence stereomicroscope (Zeiss AxioZoom.V16; Zeiss Microscopy) with a GFP filter cube.

Immunoblotting

Whole larval zebrafish were lysed in 1% Triton X-100/1× PBS by brief sonication. Proteins were resolved by electrophoresis and blotted onto PVDF membranes. We used monoclonal antibodies to detect Trc40 (1:5000; Abcam, Cambridge, MA, USA) and gamma tubulin (1:50,000, clone GTU-88; Sigma-Aldrich Corp.) and a rabbit polyclonal antibody to detect GFP (1:5000; Life Technologies). Immunoreactivity was measured with HRP-conjugated secondary antibodies (Goat anti-mouse HRP 1706516; Bio-Rad Laboratories; and Donkey anti-rabbit HRP, GENA9340v; GE Healthcare Life Sciences, Pittsburg, PA, USA) and chemiluminescent substrate (Femto Glow, Michigan Diagnostics, Royal Oak, MI, USA).

Light and Electron Microscopy

Larvae were prepared for transmission electron microscopy as previously described.[22] Semi-thin sections were made with a ultramicrotome (Leica EM UC7; Leica Microsystems, GmbH Vienna, Austria) and stained with toluidine blue and imaged with a fluorescent microscope (Carl Zeiss Microscopy). Ultrathin sectioning and TEM grid preparation was performed by the Lerner Research Institute Imaging Core. Electron microscopy was performed on a digital electron microscope (Tecnai 20, 200 kV; Philips Corp., Hillsboro, OR, USA) and micrographs acquired with an image filter and digital camera (Gatan, Inc., Pleasanton, CA, USA). Images of synaptic terminals were taken from transverse sections at the region of the optic nerve. Measurements of synaptic structures from TEM images were made in ImageJ with the ObjectJ plugin (University of Amsterdam).

Statistical Analyses

We used commercial software (Prism 6; GraphPad Software, Inc., La Jolla, CA, USA) for all statistical analyses. The statistical tests and corrections used for various analyses are provided with each experiment. Statistical significance was set at values of $P < 0.05$. Statistics are not given for nonsignificant results.

RESULTS

Mutation of *wrb* Results in Reduced Visual Function

The *wrb* (*wrb^bi1482*) mutant was previously identified in a forward genetic "shelf screen" of fish mutagenized by retroviral insertion[23,24] on the basis of a weak optokinetic response, or OKR.[13] Prior to 4 dpf, *wrb^bi1482* (referred here as *wrb^−/−*) mutants could not be distinguished morphologically from their phenotypically wild-type siblings. By 5 days post fertilization, *wrb^−/−* mutants lacked swim bladders and had slightly smaller eyes (Fig. 1A). In semi-thin plastic sections of *wrb^−/−* larvae, retinal lamination remained intact but the eyes were smaller (Fig. 1B). Acellular voids were occasionally seen in the outer nuclear layer (Fig. 1B, arrows), but this phenotype was not fully penetrant. The mutants *wrb^−/−* exhibited a reduced touch response when briefly challenged with a light touch to the tail with an insect pin; however, mutants demonstrated normal "S-bend" escape responses to stronger tail-touches or repeated stimuli, indicating that touch perception rather than locomotion was affected. Reduction in touch avoidance correlated with reduced numbers of lateral line hair cells, as the styryl dye DASPEI failed to label neuromasts of live *wrb^−/−* larvae (Fig. 1C). The mutation *wrb^−/−* resulted from insertion of retroviral DNA 65 bases within the first intron of the *wrb* gene. As measured by qRT-PCR, *wrb* mRNA expression in *wrb^−/−* mutants was reduced to less than 1% of that found in *wrb^+/+* siblings (Fig. 1D). At 5 days post fertilization, *wrb* was expressed throughout the head and trunk of wild-type larvae (Fig. 1E).

For larval zebrafish, the OKR has been used to measure parameters ranging from saccade frequency[25,26] to more sophisticated measures, such as optokinetic gain.[20] We confirmed the OKR deficit in *wrb^−/−* mutants and found that saccade frequency was reduced to ~15% of wild-type values (Fig. 1F). Next, the contrast response function was measured for 5 dpf wild-type and *wrb^−/−* larvae. For wild-type larvae, the OKR increased linearly with the log of contrast, while no consistent OKR was detected in *wrb^−/−* larvae, which resulted in a flat contrast response function (Fig. 1G). To confirm that the visual deficit was caused by mutation of *wrb,* mRNA encoding wild-type zebrafish *wrb* was injected into 1-cell embryos. No obvious morphologic or developmental defects were observed in larvae following injection of *wrb* mRNA,
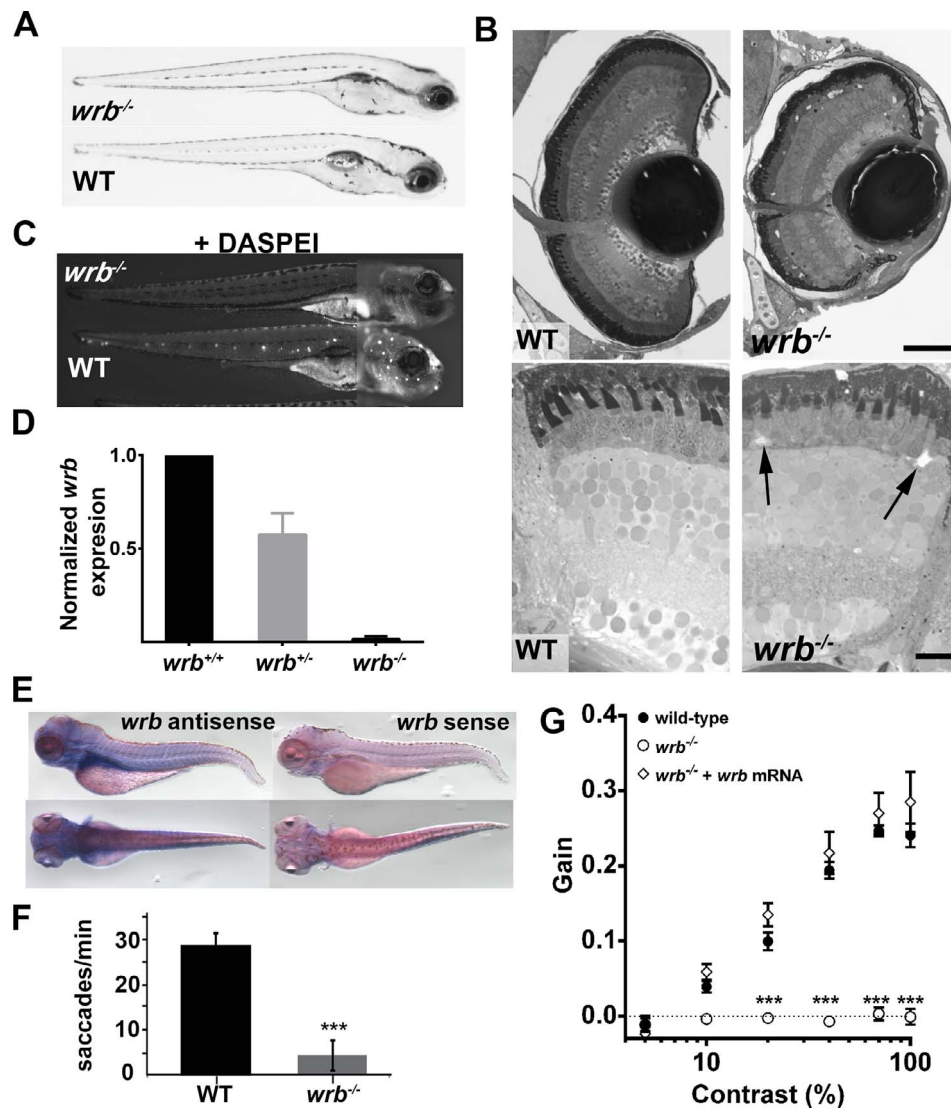
FIGURE 1. Visual system defects caused by retroviral insertion within the *wrb* gene. **(A)** Lateral views of 5 dpf *wrb*^{-/-} and wild-type larvae. **(B)** Toluidine blue–stained 1-μm thick retinal sections from 5 dpf wild-type and *wrb*^{-/-} larvae. Occasional acellular holes were observed in the ONL of *wrb*^{-/-} mutants (*arrows*). **(C)** Live 5 dpf *wrb*^{-/-} (*top*) and wild-type (*bottom*) larvae stained with the vital styryl dye DASPEI to label neuromasts. Two overlapping images, focused at the head or trunk, were stitched together for each panel. **(D)** Expression levels of *wrb* mRNA in heterozygous (*wrb*^{+/-}) and mutant (*wrb*^{-/-}) larvae at 5 dpf, compared with wild-type larvae, and normalized against beta-actin as measured by qRT-PCR. **(E)** Whole mount in situ hybridization at 5 dpf with antisense (left) and sense (right) *wrb* probes. **(F)** Saccade frequency measured from wild-type and *wrb*^{-/-} larvae at 5 dpf. **(G)** Contrast response function measured from smooth pursuit eye movements. Gain versus log contrast for 5 dpf wild-type (*black closed circles*) *wrb*^{-/-} (open circles) and *wrb*^{-/-} rescued with *wrb* mRNA (*open diamonds*). Errors bars: SEM. Significance levels are as follows: ***$P < 0.0001$. Scale bars: 50 μm (**B**, *top*) 10 μm (**B**, *bottom*).

suggesting that overexpression was tolerated. Contrast sensitivity was measured at 5 dpf and the animals were subsequently genotyped to identify wild-type and *wrb*^{-/-} mutants ($n \geq 10$ wild-type and *wrb*^{-/-}, $n = 5$ *wrb*[±] plus *wrb* mRNA). Injection of *wrb* mRNA fully restored the contrast sensitivity in *wrb*^{-/-} mutants, confirming that the OKR phenotype resulted from mutation of *wrb* (Fig. 1G).

Loss of *wrb* Leads to Diminished Synaptic Transmission Between Cones and Bipolar Cells

Abnormal OKR behavior could reflect defects at numerous points in the visual system. To determine if the reduced OKR reflected outer retina dysfunction, electroretinography (ERG) was used to measure cone-driven responses in 5 dpf zebrafish.[27] Following a 1-second flash of light, the ERG is characterized by a corneal negative a-wave originating from the photoreceptors and a corneal positive b-wave reflecting predominantly ON-bipolar electrical activity. At the end of the light stimulus, depolarization of the OFF-bipolar cells is seen in the d-wave. At dim flash intensities, the photoreceptor a-wave was more prominent in *wrb*^{-/-} mutants while the b-wave amplitudes were reduced at all amplitudes (Figs. 2A, 2B). The maximal b-wave amplitude in *wrb*^{-/-} larvae was only 20% of wild-type (Fig. 2B). It was unclear whether the reduced b-waves resulted from disrupted phototransduction or diminished synaptic transmission to ON-bipolar cells. One hour prior to ERG recordings, 5 dpf larvae were placed in fish water containing the metabotropic glutamate receptor agonist L-AP4 and the excitatory amino acid transporter inhibitor TBOA.[18,28] Drug-treated wild-type and *wrb*^{-/-} larvae exhibited an a-wave at light onset, followed by a d-wave at light offset. Quantifica-
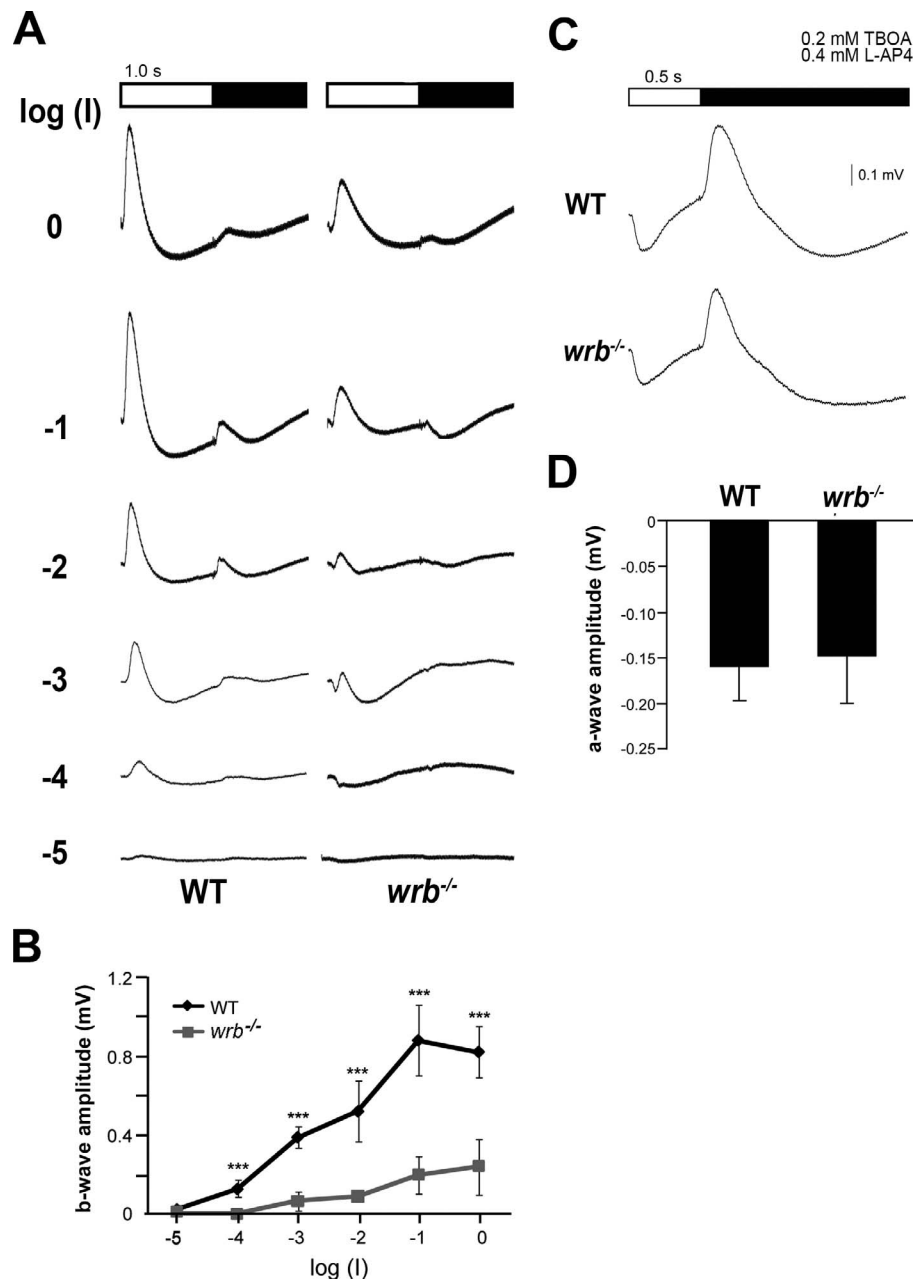
FIGURE 2. ERG reveals disrupted outer retina signaling in *wrb*$^{-/-}$ mutants. (**A**) Averaged ERG traces from wild-type and *wrb*$^{-/-}$ larval eyes elicited by a series of white flashes with onset and duration depicted at top. Flash intensity was incremented by log unit steps from bottom to top with log(I) $=-1$ corresponding to 5.3×103 μW/cm^2 at 500 nm. The interstimulus interval was 10 seconds. (**B**) Response versus stimulus functions for average peak b-wave amplitudes from wild-type and *wrb*$^{-/-}$ larvae, as measured from a-wave trough to b-wave peak. (**C**) Individual ERG traces elicited by flashes after treatment with TBOA and L-AP4 to eliminate ERG components arising from glutamate-dependent signaling. Each flash was 0.5 seconds in duration and corresponded to log(I) $=-1$ intensity. (**D**) Average a-wave maximum amplitudes from wild-type and *wrb*$^{-/-}$ larvae (*n* $= 10$, wild-type, *n* $= 10$, *wrb*$^{-/-}$). Error bars denote SEM. Significance levels are as follows: ***$P < 0.0001$.

tion of a-wave amplitudes found no difference between wild-type and *wrb*$^{-/-}$ larvae, suggesting that the reduced b-wave amplitudes in *wrb*$^{-/-}$ mutants resulted from defective transmission between cone photoreceptors and bipolar cells.

Cone Synaptic Protein Expression and Synaptic Organization in *wrb*$^{-/-}$ Larvae

To determine whether synaptic contacts between photoreceptors and bipolar cells were intact, the *Tg(nyx:mYFP)* transgenic line[14] was bred onto the *wrb* background. The *Tg(nyx.mYFP)* line uses promoter elements from the nyctalopin gene to drive expression of membrane-bound YFP in a subset of ON-bipolar cells. Fluorescence from YFP expression in bipolar cell dendrites can readily be observed in the knob-like protrusions projecting into the cone pedicles (Fig. 3A). At 5 days post fertilization, fewer protrusions were observed in *wrb*$^{-/-}$ larvae sections compared with nonmutant siblings (Figs. 3A–C; 23.5 ± 2.4 vs. 12.6 ± 2.1; *n* ≥ 4), indicating that loss of *wrb* either prevents synapse formation or leads to synapse loss. Previous work has demonstrated that cone degeneration, but not rod degeneration, leads to significant
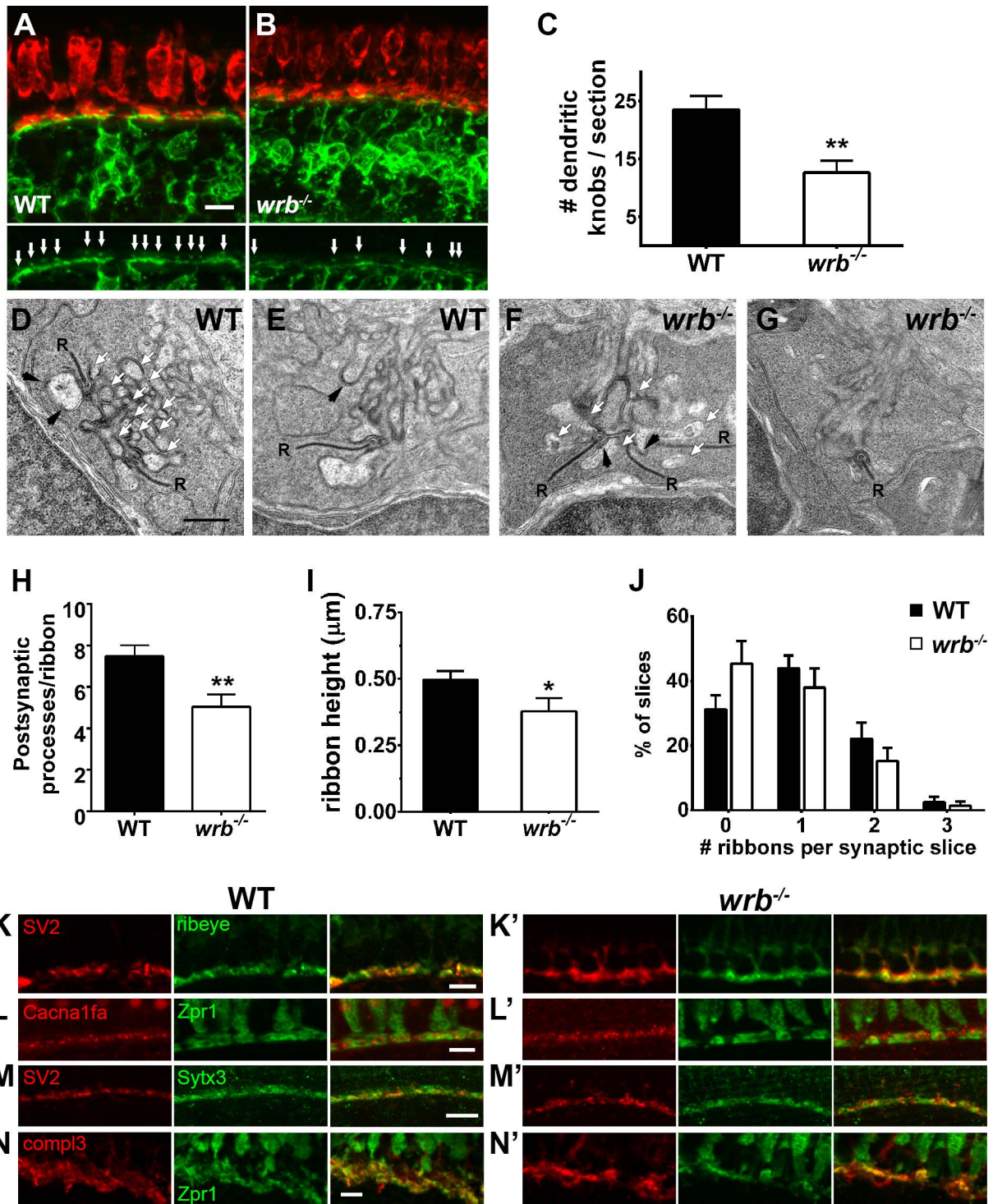
FIGURE 3. Presynaptic and postsynaptic alterations in $wrb^{-/-}$ mutant photoreceptors. (**A, B**) Representative images of the OPL from cryosections of 5 dpf *Tg(nyx:mYFP)* and $wrb^{-/-}$; *Tg(nyx:mYFP)* mutant retinas immunostained for red/green double cones (zpr1, *red*) and GFP (*green*). *Bottom panels* show bipolar dendritic projections (*white arrows*) within the OPL at higher magnification. (**C**) Quantification of dendritic invaginations inside cone pedicles across several cryosections ($n = 4$ and 8 sections for wild type and $wrb^{-/-}$, respectively). (**D–F**) Transmission electron microscopy images of cone pedicles. Synaptic ribbons (R) were surrounded by postsynaptic processes (*white arrows* denote representative processes). Horizontal cells could be identified by characteristic densities and electron-lucent cytoplasm (*black arrowheads*). Quantification of postsynaptic processes per ribbon in wild-type and mutant cone pedicles ($n = 26$ wild-type, $n = 19$ $wrb^{-/-}$ synapses). (**I**) Quantification of photoreceptor ribbon heights in wild-type and mutant synapses ($n = 32$ wild-type, $n = 18$ $wrb^{-/-}$ synapses). (**G**) Quantification of average number of synaptic terminals in which 0, 1, 2, or 3 ribbons were encountered ($n = 163$ wild-type, $n = 216$ $wrb^{-/-}$ synapses). (**H–K'**) Immunohistochemistry of 5 dpf retinal cryosections with indicated photoreceptor presynaptic markers. Images were centered at the OPL of wild-type and $wrb^{-/-}$ mutants. Cacna1fa, pore forming alpha subunit of the presynaptic L-type calcium channel; SV2, synaptic vesicle protein 2; Sytx3, photoreceptor-specific target SNARE syntaxin 3B, compl3- exocytosis regulator complexin 3. * $P < 0.05$. **$P < 0.001$. *Scale bars*: 5 μm (**A, B, H–I', K, K'**); 10 μm (**J, J'**); and 0.5 μm (**D–G**).
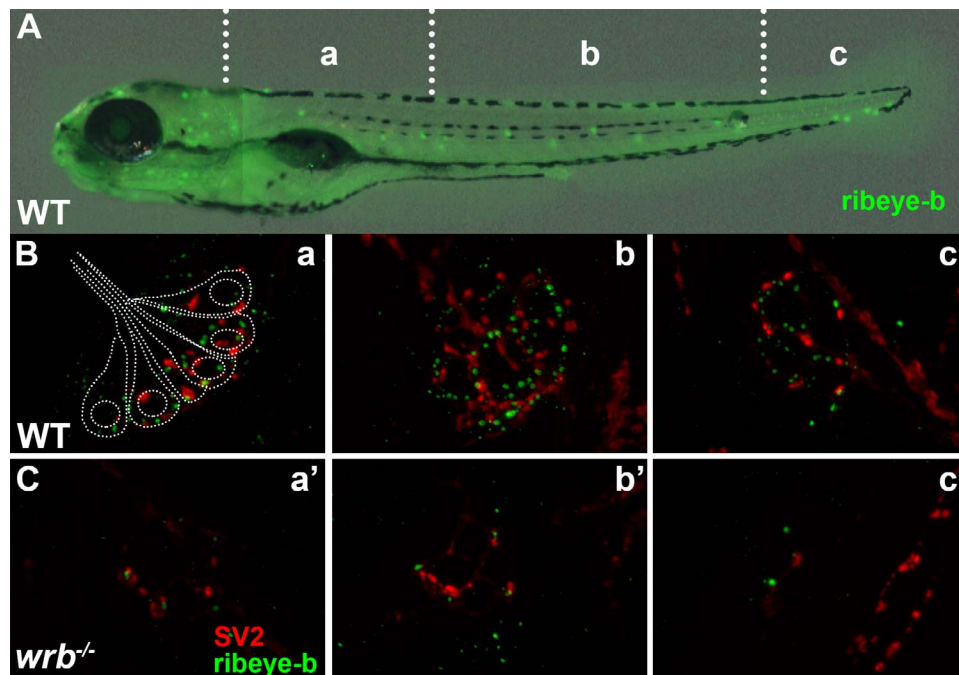
FIGURE 4. Loss of Wrb disrupts endogenous ribeye localization at synaptic ribbons in hair cells at 5 dpf. (**A**) Lateral image of 5 dpf larvae immunostained with ribeye b antibodies to label lateral line hair cells. Hair cells in *rostral* (**a**, **a'**), *middle* (**b**, **b'**), and *caudal* (**c**, **c'**) regions of the trunk were imaged by fluorescence microscopy. (**B**, **C**) Fluorescence images showing individual neuromasts immunolabeled with SV2 (*red*) and ribeye-b (*green*) antibodies in wild-type and *wrb*^{−/−} mutant larvae. *Dotted outline* in (**B**) depicts the orientation of individual hair cells within a single neuromast, as it relates to synaptic immunoreactivities.

remodeling of ON-bipolar cells in zebrafish, including ectopic dendritic projections toward photoreceptor soma, thickening and thinning of regions of the OPL, and loss of these knob-like protrusions.[29] While photoreceptor degeneration is a partially penetrant phenotype in *wrb*^{−/−} mutant, such ectopic bipolar projections were never observed.

To determine if the loss of bipolar projections reflected changes to the structure or molecular composition of *wrb*^{−/−} synapse architecture, transmission electron microscopy was used to examine photoreceptor synapses. In larval zebrafish, the cone pedicles typically contain several synaptic ribbons that denote the location of ribbon synapses.[30,31] Both horizontal cell processes and bipolar cell dendrites invaginate into the cone pedicles to form postsynaptic contacts. Horizontal cell processes flank the ribbon and appear large with electron-lucent cytoplasm, and with rounded, electron-dense patches on the postsynaptic membrane. Bipolar cell dendrites, in contrast, often appear smaller and lack the electron-dense patches of horizontal cell processes.[32] In fishes, the type I and type II on-center bipolar cells rarely make contact directly opposite the synaptic ribbon in cone pedicles, although a small process of type II on-center bipolar cells often terminates near the synaptic ribbon.[33,34] These relatively small contact areas between a cone photoreceptor and bipolar cell make the triads difficult to observe in single transverse sections.[30–32,34] Arc-shaped basal contacts form between photoreceptors and bipolar cells at the base of the pedicle and exhibit electron-dense deposits both presynaptically and postsynaptically.

A number of differences were noted in the cone pedicles of *wrb*^{−/−} mutants compared with those seen in wild-type retinas (Figs. 3D–G). Although synaptic ribbons were present and docked with arciform densities, many fewer postsynaptic processes were observed in *wrb*^{−/−} mutants (Figs. 3D, 3F; white arrows). The number of processes per synapse varied considerably, in part due to the variability in the number of synaptic ribbons at each synapse. Quantifying the number of postsynaptic processes per synaptic ribbon in several pedicles revealed a significant reduction of processes per ribbon in *wrb*^{−/−} mutants (Fig. 3H; 7.5 ± 0.5, $n = 26$, vs. 5.0 ± 0.6, $n = 19$). Most of these processes contained the electron-lucent cytoplasm and postsynaptic densities characteristic of horizontal cells. This suggests a reduction in bipolar cell processes. We next estimated the height of those ribbons with a clearly defined arciform density and flanked by obvious horizontal cell processes. We found that ribbon height was reduced by >20% in *wrb*^{−/−} mutants (Fig. 3I; 0.50 ± 0.03 μm, $n = 32$, vs. 0.38 ± 0.05 μm, $n = 18$). Next we quantified the percentage of total synapses in which 0, 1, 2, or 3 ribbons profiles were observed. There appears to be a small increase in the percentage of terminals lacking ribbon profiles in *wrb*^{−/−} images, but this difference was not significant (Fig. 3J).

We next used immunohistochemistry to examine the ribbon-specific protein ribeye and the synaptic vesicle marker SV2. The zebrafish genome contains two *ribeye* homologs, *ribeye a* and *ribeye b*, with photoreceptors exclusively expressing *ribeye b*.[35] Using polyclonal antibodies specific to ribeye b[36] and a monoclonal antibody against SV2, we consistently observed a subtle mislocalization of both proteins in *wrb*^{−/−} mutants in photoreceptors (Figs. 3K, 3K', 3M, 3M'). Hair cells of *wrb*^{−/−} mutants showed reduced ribeye b and SV2 immunoreactivities (Figs. 4A–C). Maturation of ribbon synapses requires the presence of both ribeye and L-type voltage–gated calcium channels (VGCCs), as well as VGCC activity.[37–39] Photoreceptors express the VGCC Ca$_v$1.4 (*cacna1f*) while hair cells express Ca$_v$1.3 (*cacna1d*). Reduction of ribeye disrupts the clustering of Cav1.3 on the presynaptic membrane of hair cells,[38] whereas loss of Ca$_v$1.4 leads to a significant reduction in ribeye in photoreceptors.[39,40] Despite the altered localization pattern of ribeye, Ca$_v$1.4 localized normally to the photoreceptor synapses in the *wrb*^{−/−} mutants (Figs. 3L, 3L'). Syntaxin 3B is the principal t-SNARE in ribbon-containing cells of the retina[41] and we did not observe any changes in the the

localization of synataxin-3 at the OPL of *wrb*$^{-/-}$ mutants (Figs. 3J, 3J'). Lastly, we did not observe any differences in expression of complexin3, the regulator of SNARE mediated exocytosis (Figs. 3N, 3N').

Knockdown of the Cytoplasmic ATPase Trc40 Results in a *wrb*$^{-/-}$-Like Phenotype

In yeast, Wrb functions as an ER membrane–bound receptor for Trc40 during TA protein targeting.[7,8,42] We therefore tested whether *trc40* deficiency also resulted in similar visual function and mechanotransduction phenotypes observed in *wrb*$^{-/-}$ mutants. Both translation-blocking (MO1) and splice-blocking (MO2) morpholinos knocked down *trc40* in wild-type fish and produced similar phenotypic effects. Morphants *trc40* lacked swim bladders but did not exhibit overt developmental or morphologic abnormalities through 5 dpf (Fig. 5A). To verify the specificity of *trc40* knockdown, mRNA encoding eGFP-tagged human *TRC40* was coinjected with *trc40* MO1. Morpholinos reduced levels of endogenous Trc40 protein by at least 97% at 3 to 5 dpf, while exogenous Trc40-GFP was clearly detectable at 5 dpf in morphants coinjected with mRNA (Fig. 5B). Injection of MO1 into wild-type fish resulted in reduced DASPEI labeling of lateral line hair cells, similar to the reduction observed in *wrb*$^{-/-}$ mutants. Injection of MO1 into nyx:YFP fish also recapitulated the loss of ON bipolar cell contacts at the OPL previously seen in *wrb*$^{-/-}$ mutants. Similar to *wrb*$^{-/-}$ mutants, we observed 50% fewer knob-like projections inside cone pedicles in *trc40* MO1 morphants (24.3 ± 1.5 versus 10.25 ± 2.4; $n \geq 8$; Figs. 5D, 5E). Injection of either *trc40* MO1 or MO2 also disrupted visual function similar to *wrb*$^{-/-}$ mutants and reduced OKR contrast sensitivity (Fig. 5F). Importantly, coinjection of MO1 with mRNA encoding human *TRC40-eGFP* (250 pg) completely rescued visual function, indicating a specific inhibition of *trc40* (Fig. 5G). Knockdown of *trc40* also resulted in reduced touch avoidance behavior. Only 47% of MO1 and 53% of MO2 morphants had normal touch responses at 5 dpf (data not shown).

wrb Activity and Localization in Photoreceptors Is Consistent With a Role in the GET Pathway

We hypothesized that if Wrb functions as an ER receptor in vertebrates, it must localize to the ER in photoreceptors. To determine the cellular localization of Wrb, we generated a transgenic line *(TαC:wrb-eGFP)* that expressed a Wrb-eGFP fusion protein exclusively in cones by utilizing the cone transducin promoter.[16] We stained transgenic larvae with antibodies against GFP and a marker for the ER (anti-KDEL) and found a high degree of overlap, consistent with Wrb localization to the ER membrane (Fig. 6A). We also detected Wrb-eGFP colocalizing with SV2 in synaptic processes and cone pedicles in the ONL (Fig. 6A).

Within Wrb, arginine-73 (R73) is highly conserved across all known orthologs and is required for membrane recruitment and release of TA cargo from Trc40.[43] We hypothesized that if Wrb participates in the GET pathway in zebrafish, an R73A mutation would abolish Wrb function. The optokinetic response measurements contrast sensitivity of *wrb*$^{-/-}$ larvae was partially rescued by injection of mRNA encoding a wild-type zebrafish *wrb-eGFP* fusion protein (Fig. 6B). In contrast, the OKR response was undetectable when mutants were injected with mRNA encoding *wrb*^{R73A}-*GFP* (Fig. 6C). Overexpression of *wrb*^{R73A}-*eGFP* in heterozygous animals did not have a deleterious effect on the OKR response. Finally, overexpression of wild-type *wrb-eGFP* rescued touch avoidance behavior whereas overexpression of *wrb*^{R73A}-*eGFP* did not (Fig. 6D).

The experiments above suggest that disruption of *wrb* and the GET pathway results in diminished synaptic communication and disrupted synaptic organization between photoreceptors and bipolar cells. It is not clear, however, whether the GET pathway is required in photoreceptors, bipolar cells, or both cell types. To determine if visual function specifically requires Wrb activity in photoreceptors, we measured contrast sensitivity in *wrb*$^{-/-}$ mutants carrying the *Tg(TαC:wrb-eGFP)* transgene. Optokinetic response measurements contrast sensitivity of *wrb*$^{-/-}$ mutants was substantially restored by expression of the *Tg(TαC:wrb-eGFP)* transgene in photoreceptors (Fig. 6E), thereby indicating that photoreceptor function requires Wrb.

DISCUSSION

This study uncovers a role for Wrb and the GET pathway in photoreceptor synaptic transmission in vivo. Herein, we show that Wrb and Trc40 are required for visual function and architectural integrity of photoreceptor synapses. Mutation of *wrb* resulted in diminished b-waves and disrupted contacts between cones and ON bipolar cells. We also demonstrated that knockdown of *trc40* mimicked the *wrb*$^{-/-}$ mutant phenotypes. Finally, we showed that the ability of Wrb to rescue OKR behavior in *wrb*$^{-/-}$ mutants required a conserved coil-coil domain arginine (R73) known to be critical for Trc40 docking. Our results are similar to those recently reported by Lin et al.,[44] who found a significant reduction in auditory startle responses and microphonic potentials in the inner ear of *wrb*$^{-/-}$ mutants.

Role of *wrb* in the GET Pathway

The mechanistic framework for the insertion of TA proteins destined for the secretory pathway was first elucidated in yeast.[9,45] Cytosolic targeting factor Get3 binds the transmembrane domain of nascent TA proteins and shuttles the TA cargo to the Get1/Get2 receptor complex at the ER membrane.[45–48] Targeting factors Get1 and Get2 then insert TA proteins into the ER membrane upon ATP-dependent cargo release from Get3.[9] Respectively, Wrb and Trc40 are the vertebrate homologues of Get1 and Get3.[42,49] No vertebrate homolog to Get2 exists, but CAML serves as the functional homolog.[8] Our data support the hypothesis that the GET pathway is necessary for normal visual acuity in vertebrates.

Tail-anchored proteins represent a large, diverse class of proteins that include SNAREs and the Bcl-2 family of apoptosis regulators.[50,51] Given that TA proteins are numerous and ubiquitous, why are phenotypes observed in zebrafish *wrb*$^{-/-}$ mutants apparently limited to synapse defects in photoreceptors and hair cells? First, the GET pathway is not required for viability in yeast[52] and not all TA proteins require the GET pathway.[53,54] Evidence suggests that redundant, as well as independent mechanisms for membrane targeting of TA proteins exist, including posttranslational recognition by the SRP and an Hsp70-Hsp40 pathway.[54,55] Synaptic vesicles are at least 100-fold greater in number within ribbon synapses of photoreceptors[56] and hair cells[57] compared with conventional terminals of the cortex.[58] The demand for SNARE proteins in vesicle release at ribbon synapses may be substantial and therefore cells may be more sensitive to GET pathway disruption.

Photoreceptor Function Requires an Intact GET Pathway

The precise etiology of the visual defect of *wrb*$^{-/-}$ mutants remains unclear. Although both phototransduction and synaptic vesicle release in photoreceptors require TA proteins, the
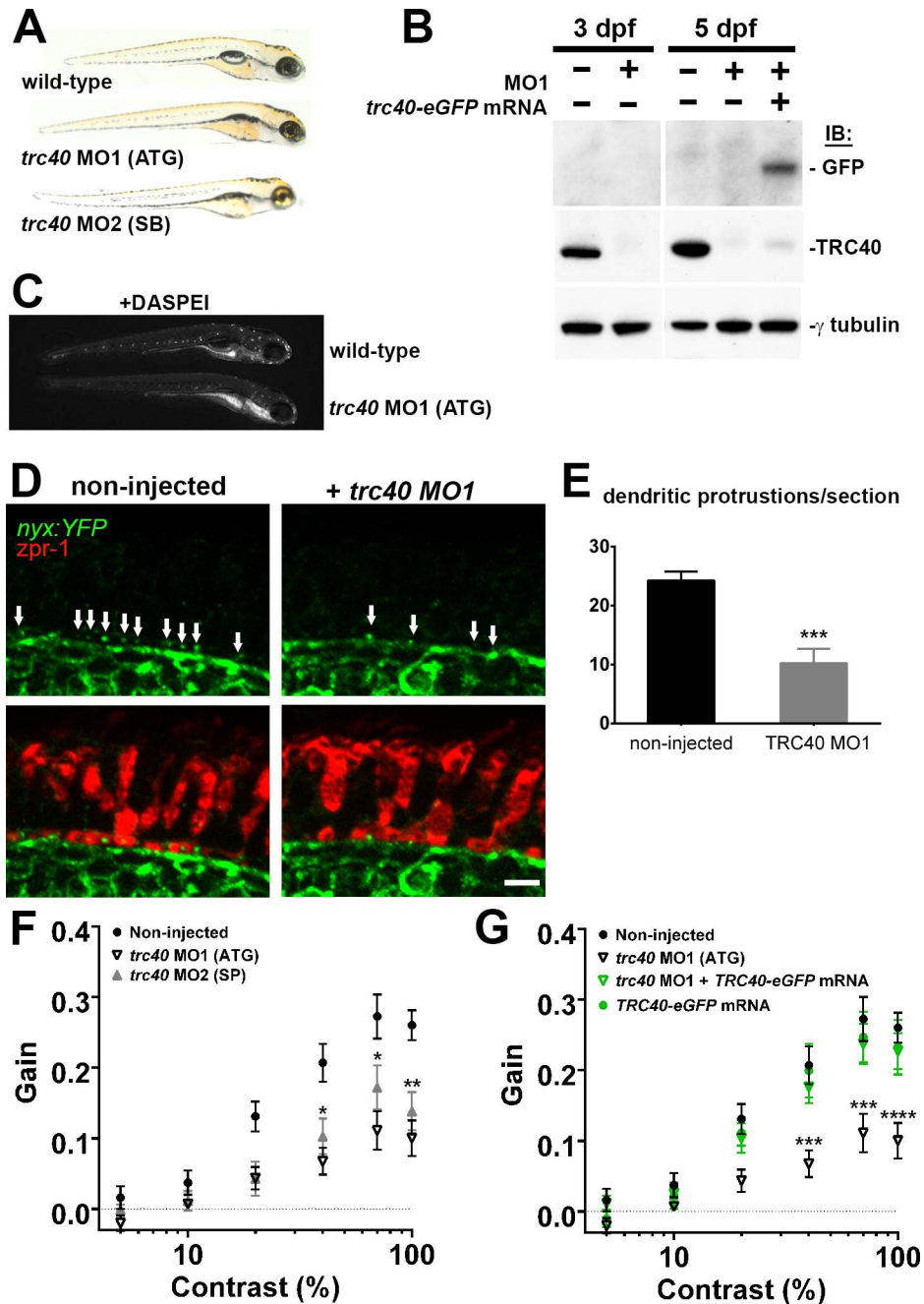
FIGURE 5. Morpholino knockdown of *trc40* results in *wrb*^{−/−}-like phenotypes. (**A**) Lateral view of 5 dpf uninjected larvae (*top*) and *trc40* MO1 (translation–blocking, ATG), and *trc40* MO2 (splice-blocking, SB) injected larvae. (**B**) Western blots of 15 μg protein lysates collected from whole larvae at 3 and 5 days after injection with 3 ng *trc40* MO1, or MO1 with human *trc40-eGFP* mRNA. Membranes were immunoblotted with antibodies to detect GFP (*top*), TRC40 (*middle*) and γ-tubulin (*bottom*). (**C**) Live 5 dpf wild-type and *trc40* morphants (MO1) larvae stained with the vital styryl dye DASPEI. (**D**) Immunohistochemistry of 5 dpf cryosections of *Tg(nyx:mYFP)* and *Tg(nyx:mYFP)* + *trc40* MO1 morphant larvae using antibodies to detect YFP (*green*) and red/green double cones (zpr1, *red*). *White arrows* indicate bipolar cell dendritic protrusions into cone pedicles. (**E**) Quantification of dendritic protrusions observed within cone pedicles from cryosections of 5 dpf larvae (*n* = 11 wild-type, 8 *trc40* MO1). (**F**) Gain of OKR versus log contrast for noninjected wild-type larvae (*closed circles*), 3 ng *trc40* MO1 morphants (*open down triangles*) and 10 ng *trc40* MO2 morphants (*filled upward triangles*) all at 5 dpf. Significance values indicated for *trc40* MO2 morphants only. (**G**) Gain of OKR versus log contrast for noninjected larvae (*filled circles*), or larvae injected with 3 ng *trc40* MO1 (*downward gray triangles*), 3 ng *trc40* MO1 + *trc40-eGFP* mRNA (*downward green triangles*) and human *trc40-eGFP* mRNA alone (*filled green circles*). Significant values noted for only for *trc40* MO1 morphants. Significance levels are as follows: *$P < 0.05$. **$P < 0.01$. ***$P < 0.001$. ****$P < 0.0001$. *Scale bar*: 5 μm.

results thus far do not directly implicate a deficit in a particular TA protein or proteins. For example, R9AP is a TA protein that binds the RGS9-Gβ5 GTPase activating complex, which is responsible for transducin inactivation.[59] Loss of R9AP or RGS9 result in delayed flash recovery of photoreceptors in mice,

which would manifest in decreased ERG waveforms.[60,61] Indeed, human mutations in *R9AP* severely repress both ERG a- and b-waves to paired flashes of light with intervals less than 10 seconds.[62] Furthermore, *R9AP* patients do not respond to low-contrast, moving stimuli. In *wrb*^{−/−} mutants, however, the
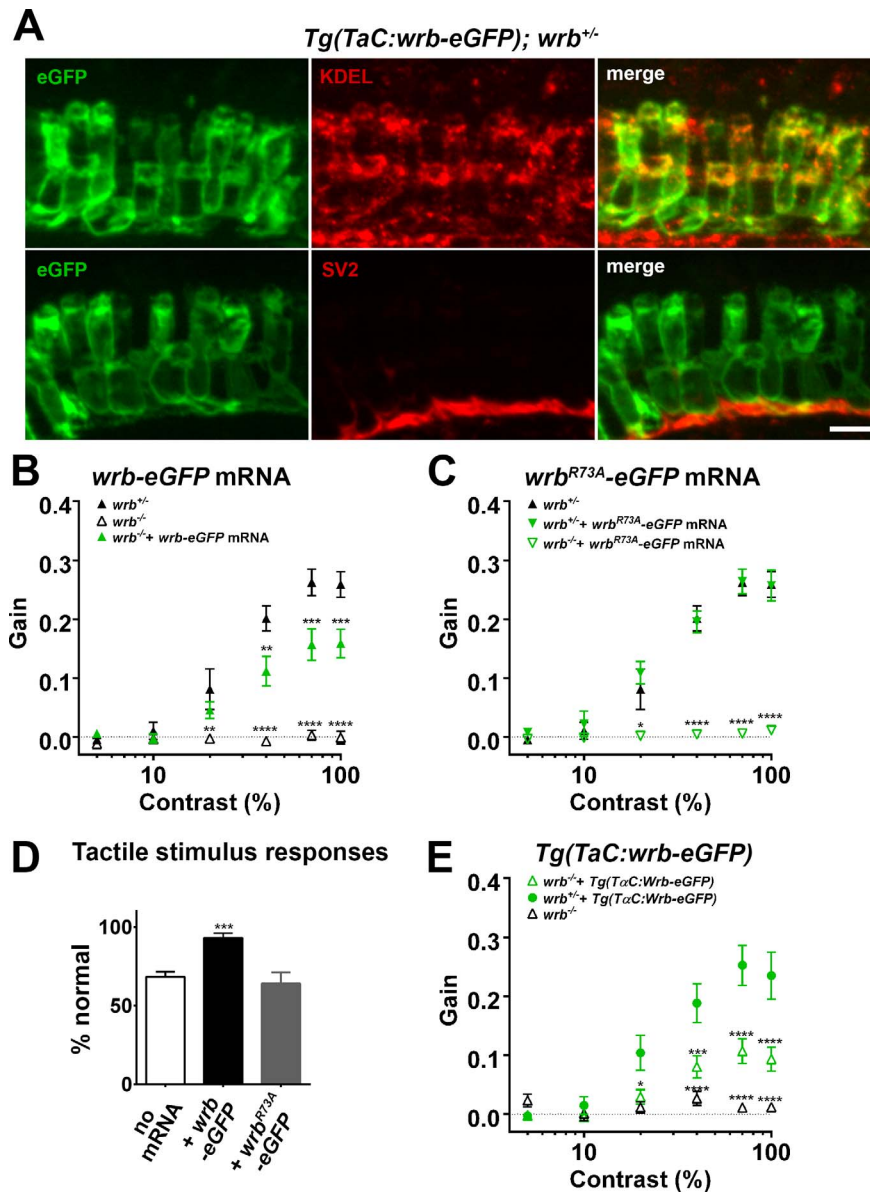
FIGURE 6. Photoreceptor *wrb* expression is critical for normal visual sensitivity. (**A**) Immunofluorescent images 10 μm-thick transverse cryosections of 5 dpf retinas from Tg(*TaC:wrb-eGFP*) stained antibodies to GFP (*green*), KDEL (*top, red*) or SV2 (*bottom, red*) to label ER and synapse respectively. (**B**) OKR gain versus log contrast plots for 5 dpf *wrb*⁺/⁻ (*closed triangles*), *wrb*⁻/⁻ mutants (*open triangles*), or *wrb*⁻/⁻ mutants injected with mRNA encoding *wrb-eGFP* (*green triangles*). (**C**) Gain of OKR versus log contrast plots for 5 dpf *wrb*⁺/⁻ heterozygous larvae (*closed triangles*), *wrb*⁺/⁻ larvae injected with mRNA encoding *wrb*^R73A^-*eGFP* (*green closed triangles*), or *wrb*⁻/⁻ mutants injected with mRNA encoding *wrb*^R73A^-*eGFP* (*green open triangles*). (**D**) Quantification of the percentage of larval offspring from a *wrb* heterozygous mating showing normal avoidance responses to light tail touch. Roughly 25% of larvae offspring (homozygous *wrb*⁻/⁻ mutants) failed to show normal responses. Almost 100% of larvae exhibited normal touch responses following injection of mRNA encoding *wrb-eGFP* into 1-cell embryos. 25% of larvae failed to show a normal response following injection of mRNA encoding *wrb*^R73A^-*eGFP*. (**E**) OKR gain versus log contrast plots from 5 dpf heterozygous and homozygous *wrb* mutants carrying the Tg(*TαC:wrb-eGFP*) transgene. *$P < 0.05$. **$P < 0.01$. ***$P < 0.001$. ****$P < 0.0001$. *Scale bar*: in (**A**): 5 μm.

ERG a-wave was intact and mutants lacked an OKR to both high and low contrast stimuli. These phenotypes were not consistent with an R9AP deficiency.

Defects in membrane insertion of SNARE proteins, a class of TA proteins, could also explain the *wrb*⁻/⁻ mutant phenotype. This was suggested by Lin et al.,[44] who reported subtle alterations in a number of tail-anchored proteins, including the SNARE protein syntaxin3. Surprisingly, our results found that expression and localization of syntaxin3 was normal in *wrb*⁻/⁻ mutants. Lin et al.[44] noted a subtle reduction in syntaxin3 expression in *wrb*⁻/⁻ mutants, although no difference in localization was mentioned. The discrepancy in expression strength may reflect a difference in the dilution or source of the syntaxin3 antibody. We cannot rule out the possibility that other SNARE proteins may be affected.

The mutant *wrb*⁻/⁻ was identified by the complete lack of OKR behavior.[13] The zebrafish requires an intact ON pathway to drive the OKR.[18,63] We show that the mutants retain a detectable light response by ERG analysis and the OFF pathway remains largely intact. This is similar to what was reported in the *nrc*⁻/⁻ mutant, which truncates the synaptojanin gene and completely disrupts synapse architecture.[18,30,64] While only mild disruptions in the distribution of ribeye and SV2 were observed in photoreceptors, the number of properly invagi-

nated ON bipolar cell dendrites was reduced in $wrb^{-/-}$ mutants. We noted a trend that $wrb^{-/-}$ photoreceptors had fewer ribbons, although this was not significant. Lin et al.[44] noted a much more significant reduction of ribbons in hair cells of the inner ear. The reduction of ON bipolar cell invaginating dendrites coincident with relatively intact presynaptic organization has been observed after mutation of both presynaptic[65] and postsynaptic[66] components. Since the b-wave is derived from ON bipolar cells, the residual ERG responses in $wrb^{-/-}$ may be mediated by the ~50% of ON bipolar cells contacting cone pedicles.

Photoreceptors require Wrb for proper function. We found that specific expression of Wrb-eGFP in cone photoreceptors restores the spatial contrast sensitivity by at least 50% (Fig. 5D), demonstrating a presynaptic requirement for Wrb in photoreceptors. This restoration was similar to that observed following global expression of Wrb-GFP via mRNA injection, but less than the recovery observed following injection of mRNA encoding untagged Wrb. This may suggest a requirement for Wrb in bipolar cells, which also contain ribbon synapses, but it is possible that the C-terminal fusion of GFP partially inhibits Wrb function by limiting access to Trc40.

Tissue Specific Roles for *wrb*

The gene *WRB* was first isolated within the region of human chromosome 21 associated with the heightened risk of congenital heart defects in Down syndrome.[67] Referred to as congenital heart disease 5 (*CHD5*), Wrb localized to the nucleus of cardiac cells. In both *Xenopus* and medaka, morpholino knockdown of *wrb* caused defects in heart chamber differentiation and cardiac looping.[12,68] In a drug sensitivity screen, zebrafish *wrb* mutants were identified as having abnormal myocardial repolarization and lower baseline heart rates, but morphologic defects were not described.[69] The function of Wrb in cardiac morphogenesis involves a nuclear association with the cardiac transcription factor CASZ1.[12] The requirement of arginine-73 for Wrb function and the similar phenotypes observed following *trc40* knockdown suggest that the visual system requires Wrb at the ER. Thus, Wrb may have tissue-specific functions in the visual system and heart, or can maintain dual functions even in the same tissue. The selectivity of the defects at sensory neuron ribbon synapses suggests unique biosynthetic demands for cells bearing ribbon synapses, but may also point to a novel role for Wrb acting through the GET pathway in synaptic function.

References

1. Deretic D, Schmerl S, Hargrave PA, Arendt A, McDowell JH. Regulation of sorting and post-Golgi trafficking of rhodopsin by its C-terminal sequence QVS(A)PA. *Proc Natl Acad Sci U S A*. 1998;95:10620–10625.

2. Kizhatil K, Baker SA, Arshavsky VY, Bennett V. Ankyrin-G promotes cyclic nucleotide-gated channel transport to rod photoreceptor sensory cilia. *Science*. 2009;323:1614–1617.

3. Zhang H, Hanke-Gogokhia C, Jiang L, et al. Mistrafficking of prenylated proteins causes retinitis pigmentosa 2. *FASEB J*. 2015;29:932–942.

4. Constantine R, Zhang H, Gerstner CD, Frederick JM, Baehr W. Uncoordinated (UNC)119: coordinating the trafficking of myristoylated proteins. *Vision Res*. 2012;75:26–32.

5. Zhang H, Constantine R, Vorobiev S, et al. UNC119 is required for G protein trafficking in sensory neurons. *Nat Neurosci*. 2011;14:874–880.

6. Hegde RS, Keenan RJ. Tail-anchored membrane protein insertion into the endoplasmic reticulum. *Nat Rev Mol Cell Biol*. 2011;12:787–798.

7. Vilardi F, Stephan M, Clancy A, Janshoff A, Schwappach B. WRB and CAML are necessary and sufficient to mediate tail-anchored protein targeting to the ER membrane. *PLoS One*. 2014;9:e85033.

8. Yamamoto Y, Sakisaka T. Molecular machinery for insertion of tail-anchored membrane proteins into the endoplasmic reticulum membrane in mammalian cells. *Mol Cell*. 2012;48: 387–397.

9. Wang F, Chan C, Weir NR, Denic V. The Get1/2 transmembrane complex is an endoplasmic-reticulum membrane protein insertase. *Nature*. 2014;512:441–444.

10. Mukhopadhyay R, Ho YS, Swiatek PJ, Rosen BP, Bhattacharjee H. Targeted disruption of the mouse Asna1 gene results in embryonic lethality. *FEBS Lett*. 2006;580:3889–3894.

11. Tran DD, Russell HR, Sutor SL, van Deursen J, Bram RJ. CAML is required for efficient EGF receptor recycling. *Dev Cell*. 2003;5:245–256.

12. Sojka S, Amin NM, Gibbs D, Christine KS, Charpentier MS, Conlon FL. Congenital heart disease protein 5 associates with CASZ1 to maintain myocardial tissue integrity. *Development*. 2014;141:3040–3049.

13. Gross JM, Perkins BD, Amsterdam A, et al. Identification of zebrafish insertional mutants with defects in visual system development and function. *Genetics*. 2005;170:245–261.

14. Schroeter EH, Wong RO, Gregg RG. In vivo development of retinal ON-bipolar cell axonal terminals visualized in nyx::-MYFP transgenic zebrafish. *Vis Neurosci*. 2006;23:833–843.

15. Kwan KM, Fujimoto E, Grabher C, et al. The Tol2kit: a multisite gateway-based construction kit for Tol2 transposon transgenesis constructs. *Dev Dyn*. 2007;236:3088–3099.

16. Kennedy BN, Alvarez Y, Brockerhoff SE, et al. Identification of a zebrafish cone photoreceptor-specific promoter and genetic rescue of achromatopsia in the nof mutant. *Invest Ophthalmol Vis Sci*. 2007;48:522–529.

17. Jowett T. Double in situ hybridization techniques in zebrafish. *Methods*. 2001;23:345–358.

18. Emran F, Rihel J, Adolph AR, Wong KY, Kraves S, Dowling JE. OFF ganglion cells cannot drive the optokinetic reflex in zebrafish. *Proc Natl Acad Sci U S A*. 2007;104:19126–19131.

19. Mueller KP, Schnaedelbach OD, Russig HD, Neuhauss SC. VisioTracker, an innovative automated approach to oculomotor analysis. *J Vis Exp*. 2011;12:3556.

20. Rinner O, Rick JM, Neuhauss SC. Contrast sensitivity, spatial and temporal tuning of the larval zebrafish optokinetic response. *Invest Ophthalmol Vis Sci*. 2005;46:137–142.

21. Schneider CA, Rasband WS, Eliceiri KW. NIH Image to ImageJ: 25 years of image analysis. *Nat Methods*. 2012;9:671–675.

22. Sukumaran S, Perkins BD. Early defects in photoreceptor outer segment morphogenesis in zebrafish ift57, ift88 and ift172 Intraflagellar Transport mutants. *Vision Res*. 2009;49:479–489.

23. Amsterdam A, Burgess S, Golling G, et al. A large-scale insertional mutagenesis screen in zebrafish. *Genes Dev*. 1999;13:2713–2724.

24. Amsterdam A, Nissen RM, Sun Z, Swindell EC, Farrington S, Hopkins N. Identification of 315 genes essential for early zebrafish development. *Proc Natl Acad Sci U S A*. 2004;101: 12792–12797.

25. Brockerhoff SE, Hurley JB, Janssen-Bienhold U, Neuhauss SC, Driever W, Dowling JE. A behavioral screen for isolating zebrafish mutants with visual system defects. *Proc Natl Acad Sci U S A*. 1995;92:10545–10549.

26. Easter SS Jr, Nicola GN. The development of vision in the zebrafish (Danio rerio). *Dev Biol*. 1996;180:646–663.

27. Bilotta J, Saszik S, Sutherland SE. Rod contributions to the electroretinogram of the dark-adapted developing zebrafish. *Dev Dyn*. 2001;222:564–570.

28. Wong KY, Gray J, Hayward CJ, Adolph AR, Dowling JE. Glutamatergic mechanisms in the outer retina of larval zebrafish: analysis of electroretinogram b- and d-waves using a novel preparation. *Zebrafish*. 2004;1:121–131.

29. Saade CJ, Alvarez-Delfin K, Fadool JM. Rod photoreceptors protect from cone degeneration-induced retinal remodeling and restore visual responses in zebrafish. *J Neurosci*. 2013;33: 1804–1814.

30. Allwardt BA, Lall AB, Brockerhoff SE, Dowling JE. Synapse formation is arrested in retinal photoreceptors of the zebrafish nrc mutant. *J Neurosci*. 2001;21:2330–2342.

31. Stell WK, Ishida AT, Lightfoot DO. Structural basis for on-and off-center responses in retinal bipolar cells. *Science*. 1977;198: 1269–1271.

32. Stell WK. The structure and relationships of horizontal cells and photoreceptor-bipolar synaptic complexes in goldfish retina. *Am J Anat*. 1967;121:401–423.

33. Saito T, Kujiraoka T, Yonaha T, Chino Y. Reexamination of photoreceptor-bipolar connectivity patterns in carp retina: HRP-EM and Golgi-EM studies. *J Comp Neurol*. 1985;236:141–160.

34. Klooster J, Yazulla S, Kamermans M. Ultrastructural analysis of the glutamatergic system in the outer plexiform layer of zebrafish retina. *J Chem Neuroanat*. 2009;37:254–265.

35. Wan L, Almers W, Chen W. Two ribeye genes in teleosts: the role of Ribeye in ribbon formation and bipolar cell development. *J Neurosci*. 2005;25:941–949.

36. Obholzer N, Wolfson S, Trapani JG, et al. Vesicular glutamate transporter 3 is required for synaptic transmission in zebrafish hair cells. *J Neurosci*. 2008;28:2110–2118.

37. Zabouri N, Haverkamp S. Calcium channel-dependent molecular maturation of photoreceptor synapses. *PLoS One*. 2013;8: e63853.

38. Sheets L, Trapani JG, Mo W, Obholzer N, Nicolson T. Ribeye is required for presynaptic Ca(V)1.3a channel localization and afferent innervation of sensory hair cells. *Development*. 2011; 138:1309–1319.

39. Jia S, Muto A, Orisme W, et al. Zebrafish Cacna1fa is required for cone photoreceptor function and synaptic ribbon formation. *Hum Mol Genet*. 2014;23:2981–2994.

40. Liu X, Kerov V, Haeseleer F, et al. Dysregulation of Ca(v)1.4 channels disrupts the maturation of photoreceptor synaptic ribbons in congenital stationary night blindness type 2. *Channels (Austin)*. 2013;7:514–523.

41. Curtis LB, Doneske B, Liu X, Thaller C, McNew JA, Janz R. Syntaxin 3b is a t-SNARE specific for ribbon synapses of the retina. *J Comp Neurol*. 2008;510:550–559.

42. Vilardi F, Lorenz H, Dobberstein B. WRB is the receptor for TRC40/Asna1-mediated insertion of tail-anchored proteins into the ER membrane. *J Cell Sci*. 2011;124:1301–1307.

43. Wang F, Whynot A, Tung M, Denic V. The mechanism of tail-anchored protein insertion into the ER membrane. *Mol Cell*. 2011;43:738–750.

44. Lin SY, Vollrath MA, Mangosing S, Shen J, Cardenas E, Corey DP. The zebrafish pinball wizard gene encodes WRB, a tail-anchored-protein receptor essential for inner-ear hair cells and retinal photoreceptors. *J Physiol*. 2016;594:895–914.

45. Schuldiner M, Metz J, Schmid V, et al. The GET complex mediates insertion of tail-anchored proteins into the ER membrane. *Cell*. 2008;134:634–645.

46. Mariappan M, Mateja A, Dobosz M, Bove E, Hegde RS, Keenan RJ. The mechanism of membrane-associated steps in tail-anchored protein insertion. *Nature*. 2011;477:61–66.

47. Rome ME, Rao M, Clemons WM, Shan SO. Precise timing of ATPase activation drives targeting of tail-anchored proteins. *Proc Natl Acad Sci U S A*. 2013;110:7666–7671.

48. Stefer S, Reitz S, Wang F, et al. Structural basis for tail-anchored membrane protein biogenesis by the Get3-receptor complex. *Science*. 2011;333:758–762.

49. Stefanovic S, Hegde RS. Identification of a targeting factor for posttranslational membrane protein insertion into the ER. *Cell*. 2007;128:1147–1159.

50. Borgese N, Brambillasca S, Colombo S. How tails guide tail-anchored proteins to their destinations. *Curr Opin Cell Biol*. 2007;19:368–375.

51. Kalbfleisch T, Cambon A, Wattenberg BW. A bioinformatics approach to identifying tail-anchored proteins in the human genome. *Traffic*. 2007;8:1687–1694.

52. Schuldiner M, Collins SR, Thompson NJ, et al. Exploration of the function and organization of the yeast early secretory pathway through an epistatic miniarray profile. *Cell*. 2005;123: 507–519.

53. Borgese N, Gazzoni I, Barberi M, Colombo S, Pedrazzini E. Targeting of a tail-anchored protein to endoplasmic reticulum and mitochondrial outer membrane by independent but competing pathways. *Mol Biol Cell*. 2001;12:2482–2496.

54. Rabu C, High S. Membrane protein chaperones: a new twist in the tail? *Curr Biol*. 2007;17:R472–R474.

55. Abell BM, Pool MR, Schlenker O, Sinning I, High S. Signal recognition particle mediates post-translational targeting in eukaryotes. *EMBO J*. 2004;23:2755–2764.

56. Heidelberger R, Thoreson WB, Witkovsky P. Synaptic transmission at retinal ribbon synapses. *Prog Retin Eye Res*. 2005; 24:682–720.

57. Lenzi D, Runyeon JW, Crum J, Ellisman MH, Roberts WM. Synaptic vesicle populations in saccular hair cells reconstructed by electron tomography. *J Neurosci*. 1999;19:119–132.

58. Wilhelm BG, Mandad S, Truckenbrodt S, et al. Composition of isolated synaptic boutons reveals the amounts of vesicle trafficking proteins. *Science*. 2014;344:1023–1028.

59. Hu G, Wensel TG. R9AP, a membrane anchor for the photoreceptor GTPase accelerating protein, RGS9-1. *Proc Natl Acad Sci U S A*. 2002;99:9755–9760.

60. Keresztes G, Martemyanov KA, Krispel CM, et al. Absence of the RGS9.Gbeta5 GTPase-activating complex in photoreceptors of the R9AP knockout mouse. *J Biol Chem*. 2004;279: 1581–1584.

61. Lyubarsky AL, Naarendorp F, Zhang X, Wensel T, Simon MI, Pugh EN Jr. RGS9-1 is required for normal inactivation of mouse cone phototransduction. *Mol Vis*. 2001;7:71–78.

62. Nishiguchi KM, Sandberg MA, Kooijman AC, et al. Defects in RGS9 or its anchor protein R9AP in patients with slow photoreceptor deactivation. *Nature*. 2004;427:75–78.

63. Sugita Y, Miura K, Araki F, Furukawa T, Kawano K. Contributions of retinal direction-selective ganglion cells to optokinetic responses in mice. *Eur J Neurosci*. 2013;38:2823–2831.

64. Van Epps HA, Hayashi M, Lucast L, et al. The zebrafish nrc mutant reveals a role for the polyphosphoinositide phosphatase synaptojanin 1 in cone photoreceptor ribbon anchoring. *J Neurosci*. 2004;24:8641–8650.

65. Sato S, Omori Y, Katoh K, et al. Pikachurin, a dystroglycan ligand, is essential for photoreceptor ribbon synapse formation. *Nat Neurosci*. 2008;11:923–931.

66. Cao Y, Masuho I, Okawa H, et al. Retina-specific GTPase accelerator RGS11/G beta 5S/R9AP is a constitutive heterotrimer selectively targeted to mGluR6 in ON-bipolar neurons. *J Neurosci*. 2009;29:9301–9313.

67. Egeo A, Mazzocco M, Sotgia F, et al. Identification and characterization of a new human cDNA from chromosome 21q22.3 encoding a basic nuclear protein. *Hum Genet*.1998; 102:289–293.

68. Murata K, Degmetich S, Kinoshita M, Shimada E. Expression of the congenital heart disease 5/tryptophan rich basic protein homologue gene during heart development in medaka fish, Oryzias latipes. *Dev Growth Differ*. 2009;51:95–107.

69. Milan DJ, Kim AM, Winterfield JR, et al. Drug-sensitized zebrafish screen identifies multiple genes, including GINS3, as regulators of myocardial repolarization. *Circulation*. 2009; 120:553–559.